

Development of superconducting tunnel junction photon detector on SOI preamplifier board to search for radiative decays of cosmic background neutrino

Kota Kasahara*, Shin-Hong Kim, Yuji Takeuchi, Ren Senzaki, Kazuki Nagata, Takuya Okudaira, Masahiro Kanamaru, Tatsuya Ichimura, Koya Moriuchi, Kenji Kiuchi, Yasuo Arai¹, Masashi Hazumi¹, Hirokazu Ikeda², Shuji Matsuura², Takehiko Wada², Satoru Mima³, Hirokazu Ishino⁴, Takuo Yoshida⁵, Yukihiko Kato⁶, Erik Ramberg⁷, Mark Kozlovsky⁷, Paul Ruvinov⁷, Dmitri Segratskov⁷

University of Tsukuba, Ibaraki 305-8571, Japan

¹*KEK, Ibaraki 305-0801, Japan*

²*JAXA ISAS, Kanagawa 252-5210, Japan*

³*RIKEN, Saitama 351-0198, Japan*

⁴*Okayama University, Okayama 700-8530, Japan*

⁵*University of Fukui, Fukui 910-8507, Japan*

⁶*Kinki University, Osaka 577-8502, Japan*

⁷*Fermi National Accelerator Laboratory, Illinois, 60510, US*

E-mail: kasahara@hep.px.tsukuba.ac.jp

We present a development of a novel photon detector based on superconducting tunnel junction (STJ) and silicon-on-Insulator (SOI) technology for application to an experiment to search for radiative decays of cosmic background neutrinos using photon energy spectrum in the cosmic infrared background region. The requirement of the detector for the experiment is a capability of photon-by-photon detection in the far-infrared region. In principle, a Nb/Al-STJ is expected to be able to detect a single far-infrared photon, however, it has not succeeded yet even with the STJ since the signal from the single far-infrared photon is much smaller than the readout noise level currently achieved. To solve this problem, we employ a preamplifier that can be operated at a cryogenic temperature below 1K to improve the signal-to-noise ratio in STJ readout signal. SOI preamplifier is a promising candidate as it was reprocessed to function at 4K by a JAXA and KEK group. We process a STJ directly on the SOI wafer with the preamplifier circuit to make the detector simple and compact. First we tested a STJ on a SOI board only with SOI-MOSFETs to verify the electrical contact between the STJ and the SOIFET electrodes as well as the STJ being processed without causing any damage on SOI-FET. We have confirmed that the SOI-FET shows an excellent performance below 1K and the STJ on the SOI can operate normally. Then we designed a more practical version of the SOI-STJ photon detector with a preamplifier circuit in the SOI wafer.

Technology and Instrumentation in Particle Physics 2014,

2-6 June, 2014

Amsterdam, the Netherlands

*Speaker.

1. Search for radiative decays of cosmic background neutrinos

The mass-square differences between neutrino generations, Δm^2 , Δm_{32}^2 and Δm_{21}^2 were measured to be $(2.32^{+0.12}_{-0.08}) \times 10^{-3} \text{ eV}^2$ and $(7.50 \pm 0.20) \times 10^{-5} \text{ eV}^2$, respectively, by various neutrino oscillation experiments [1]. However, the neutrino mass itself has not been measured yet. We aim at measuring the neutrino mass itself with the neutrino radiative decay.

The photon energy from the neutrino radiative decay ($\nu_3 \rightarrow \nu_2 + \gamma$) in the ν_3 rest frame is described as the following equation:

$$E_\gamma = \frac{m_3^2 - m_2^2}{2m_3}, \quad (1.1)$$

where E_γ is the photon energy from the neutrino radiative decay, and m_3 and m_2 are the heaviest and the second heaviest neutrino masses, respectively. The numerator has been measured by the oscillation experiments, therefore, the measurement of the photon energy enables us to determine the neutrino mass itself. The neutrino lifetime is expected to be very long ($\tau_3 = O(10^{43})$ years) in the standard model [2]. However, in the left-right symmetric model, which is described in $SU(2)_L \otimes SU(2)_R \otimes U(1)_{B-L}$ symmetry group, the lifetime is allowed to be $\tau_3 = O(10^{17})$ years [3] in the shortest.

The most promising method is to observe the photon from the decay of the cosmic background neutrino, which has a temperature of 1.9K and a particle density ρ of 110 cm^{-3} per generation. The detection of the neutrino decay also indicates an experimental discovery of the cosmic background neutrino which is only predicted by the standard cosmology.

The expected photon energy from the neutrino radiative decay is about 25 meV assuming $m_3 = 50 \text{ meV}$. In this energy region, the largest background is the zodiacal emission. To estimate the requirement for the energy resolution of the photon detector, we performed a simulation study on the assumption of $m_3 = 50 \text{ meV}$, $m_2 = 10 \text{ meV}$ and $\tau_3 = 1.5 \times 10^{17}$ years. In this simulation, we also assume a 20 cm-diameter telescope with a viewing angle of 0.1 degrees, a photon detector of 100 % detection efficiency with the energy resolution from 0 % to 5 %, and 10-hour measurement. Figure 1 shows the resulting photon energy spectrum from the cosmic background neutrino decay together with the predicted zodiacal emission. The photon energy spectrum from neutrino radiative decay has a sharp edge at the expected photon energy from ν_3 at rest and the tail in the lower energy region due to the red shift effect. To detect the neutrino radiative decay significantly in such a large background, it is found the photon detector is required to have 2 % energy resolution at the edge.

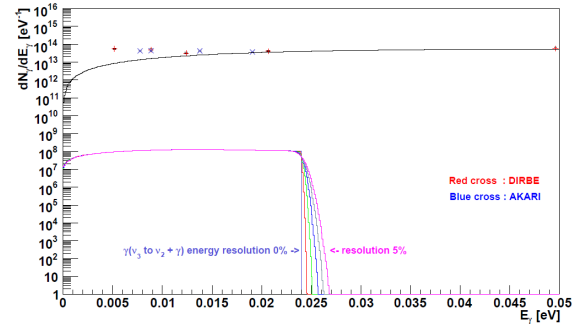


Figure 1: The photon energy spectrum of the zodiacal emission and neutrino radiative decay on the assumption of the detector with each energy resolution from 0 % to 5 %. The zodiacal emission is described as a theoretical function of the black-body radiation. The cross and plus marks show the data from DIRBE and AKARI measurements. $\tau_3 = 1.5 \times 10^{17}$ years for the neutrino lifetime and $m_3 = 50 \text{ meV}$ are assumed.

We plan to perform a rocket experiment, aiming at improving the current experimental lower limit to the neutrino lifetime by two orders of magnitude in a 5-minute measurement [4, 5]. We deploy 8 spectrometers each of which consists of an array of 50 Nb/Al-STJ pixels, and a diffraction grating is adopted to separate photons according to their wavelengths across the pixel array to measure the photon energy in the range from 15 meV to 31 meV ($\lambda = 40 - 80 \mu\text{m}$).

2. Introduction to superconducting tunnel junction

The superconducting tunnel junction (STJ), also known as a Josephson junction, where consists of two superconductors separated by a very thin insulator layer is shown in Fig. 2. The typical time constant of the Nb/Al-STJ signal is a few micro seconds. It originates in the diffusion time of quasi-particles and faster than the bolometer such as the transition edge sensor (TES), which is one of traditional superconducting detectors. By using a narrow time window for the STJ signal charge collection, signal-to-noise ratio is expected to be improved.

In the superconducting tunnel junction, excited electrons (quasi-particles) above their energy gap tunnel through the potential barrier by the thin insulator layer due to the tunnel effect. By measuring the tunnel current of quasi-particles excited by an incident particle, we can measure the energy of the particle. The number of quasi-particles in Nb/Al-STJ is given as the following equation:

$$N_q = G_{\text{Al}} \frac{E_\gamma}{1.7\Delta}, \quad (2.1)$$

where G_{Al} is a gain arising from the difference between gap energies of two superconducting layers (Nb : 1.550 meV, Al : 0.172 meV), E_γ is the absorbed energy of the incident particle, Δ is the superconducting gap energy of niobium. For example, the number of quasi-particles created by a single photon of 25 meV in Nb/Al-STJ is corresponding to about 100 electrons assuming $G_{\text{Al}} = 10$.

3. Cold preamplifier

We confirmed that a Nb/Al-STJ with $4 \mu\text{m}^2$ junction size can detect a visible light ($\lambda = 465 \text{ nm}$) at a single photon level and found a separation of the single photon signal from the pedestal noise is at the level of 0.4σ significance.

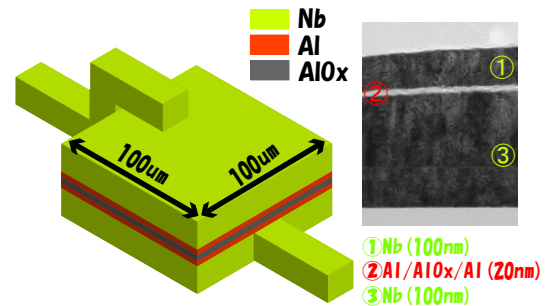


Figure 2: Schematic draw of the Nb/Al-STJ (left) and the cross-section image of a Nb/Al-STJ with a transmission electron microscope (right)

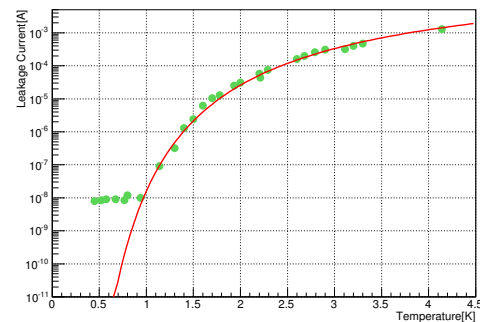


Figure 3: Temperature dependence of the leakage current for a Nb/Al-STJ ($100\mu\text{m} \times 100\mu\text{m}$). Measured data (dots) and the theoretical prediction (solid curve) are shown.

As we aim at 5σ separation for a single far-infrared photon signal from the pedestal noise, we need further improvement by a low-noise preamplifier working at the operation temperature of the Nb/Al-STJ. Requirements for the amplifier are divided into roughly the following three categories:

First, the amplifier should be operated below 800 mK. The leakage current of the Nb/Al-STJ is required to be below 100 pA to separate the signal from the shot noise from the leakage current. The leakage current is practically caused by defects such as pinholes in the insulation layer as well as thermal excitation of cooper pairs. The temperature dependence of the leakage current is shown in Fig. 3. The solid curve shows theoretical prediction of the leakage current originating in the thermal excitation in the BCS theory. The measured data differs from the predicted curve below 1 K because of the leakage current which arises from the defects. We expect to be able to reduce the pinholes by using a smaller junction size. Meanwhile, to reduce the thermal excitation, we need to operate STJ below 800 mK, and thus the amplifier is required to be at the same temperature.

Second, the total power consumption of the STJ and preamplifiers must be below the cooling power of the refrigerator. Accordingly, it is desirable to keep the power consumption in the amplifier to be as low as possible.

Finally, since the time constant of the Nb/Al-STJ signal is a few μ s, the gain of the amplifier is required to be sufficiently high up to 1 MHz.

3.1 Silicon-on-Insulator devices

The Silicon-On-Insulator (SOI) amplifier is a candidate for readout of the Nb/Al-STJ. It has been reported to operate at 4K by a JAXA/KEK group [6]. The large scale integration (LSI) on SiO₂ insulator has been developed with the SOI technology. The LSI on the insulation layer enables denser integration of FETs than the conventional bulk-FETs. The SOI-based device is possible to reduce parasitic capacitance among MOSFETs and the substrate. The smaller parasitic capacitance benefits operation with lower power consumption and at higher speed. FD (fully-depleted) -SOI-FET, which has a very thin channel layer (about 50 nm), further reduces the capacitance and enhances these advantages. Furthermore, FD-SOI-FET does not have malfunctions such as kink, hysteresis and so on which arise from surplus high mobility carriers created at ultra-low temperature in case of highly doped MOS-FET.

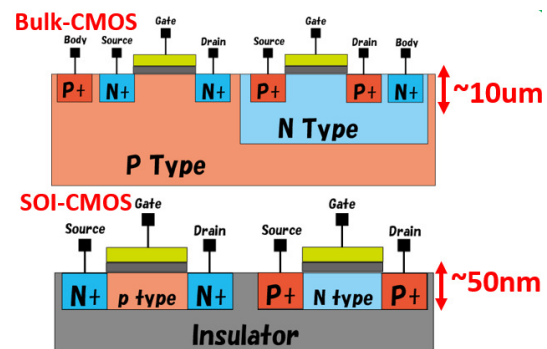


Figure 4: Schematic draws of the typical bulk-FET and SOI-FET

4. Development of the SOI-STJ photon detector

Hereafter we refer to the device where a Nb/Al-STJ is formed directly on a SOI chip in which the preamplifier circuit is integrated as the SOI-STJ photon detector. The SOI-STJ photon detector can derive many benefits from the advantages in the SOI technology. It is expected to improve signal-to-noise ratio as well as a potential for expansion to a multi-pixel device.

As the first step, we tested the Nb/Al-STJ on the SOI board which includes only MOSFET to answer the following questions: Whether SOI-FETs suffer any damage during process of the STJ, whether quality of the Nb/Al-STJ even on the SOI board is sufficiently good, and so on. The schematics and the photo-micrograph of the first prototype of the SOI-STJ are shown in Fig. 5 and Fig. 6, respectively.

4.1 Performance of Nb/Al-STJ processed on SOI board

We measured a current-voltage relation (I-V curve) of a Nb/Al-STJ with the size of $50 \mu\text{m} \times 50 \mu\text{m}$ processed on a SOI board at 700 mK with a dilution refrigerator. The I-V curve shows a DC Josephson current which is confirmed to be suppressed after applying a magnetic field of 35 Gauss parallel to the insulator plane as shown in Fig. 8. The leakage current, which is defined as the current at operation voltage 0.5 mV, is found to be around 6 nA. This indicates the STJ on the SOI board has a similar performance to the best of the nominal Nb/Al-STJ samples which is processed on a Si wafer and measured to be the leakage current of 10 nA (see Fig. 3).

We also observed the response of a Nb/Al-STJ processed on a SOI board to a pulsed laser light of 465 nm as shown in Fig. 7. The time constant of the signal is found to be about $1 \mu\text{s}$. It implies that the signal is originating from the quasi-particles and their diffusion.

4.2 Performance of SOI-FET at ultra-low temperature

We also measured I-V curves of SOI-FETs after processing Nb/Al-STJs at an ultra-low temperature. The measured I-V curves are shown in Fig. 9a and Fig. 9b. Both the nMOSFET and the pMOSFET are confirmed to function below 800 mK. Fig. 9c and Fig. 9d show the the trans-conductance g_m , which is proportional to the gain, as a function of V_{ds} at each temperature of room, the liquid helium and lower. The plots indicate g_m at the operation voltage ($V_{ds} = 0.2 \text{ V}$) is not so sensitive to the temperature, and we can employ the SOI-FET for CMOS amplifier which is operated with low power consumption at the cryogenic temperature.

We investigated the SOI-FETs with different dimensions in the channel width and the channel length as well (ranging from $1 \mu\text{m}$ to $1000 \mu\text{m}$), and found we can control the drain current at the operation voltages. This means that we can adjust the power consumption of the cold amplifier. Figure 10 shows the I-V curve of the SOIFET with the smallest power consumption in the FETs we measured. In this case, the power consumption at the operation point $V_{ds} = 0.5 \text{ V}$ and $V_{gs} = 0.8 \text{ V}$ in the saturation region is found to be 45 nW from Fig. 10b. The SOI-FET thus can operate with

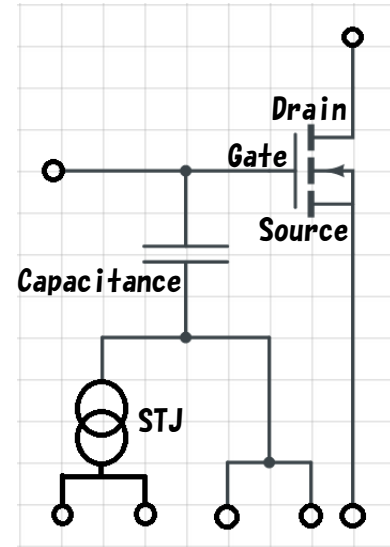


Figure 5: Schematics of the first prototype SOI-STJ

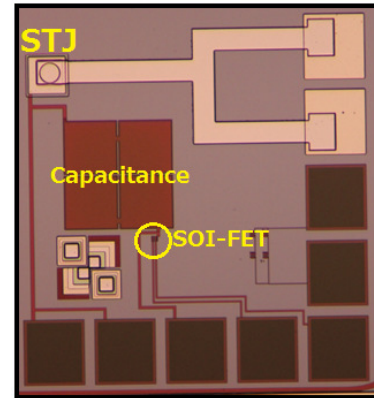


Figure 6: A photo-micrograph of the first prototype SOI-STJ

comparative small power consumption and is consequently expected to be suitable for our application.

We, however, need to evaluate the thermal model of our apparatus first and clarify the requirement for the power consumption in the amplifier. We are also examining a possible improvement for FET with higher gain and lower power consumption in exchange of the response speed by using FET around the threshold voltage.

Due to the large output impedance in the first prototype, capacitance in the external readout cable hinders to estimate the amplifier response in the high frequency region above the order of kHz. We are updating the SOI-STJ design for the readout of the amplified Nb/Al-STJ signal via the external cable. The new design of the SOI-STJ is shown in Fig. 11. In the new design, we adopt the CMOS amplifier since it is confirmed that both of nMOS and pMOS are available at the cryogenic temperature, and integrate the follower stage where the output impedance is reduced to transmit the output signal in higher frequency region to the external cable.

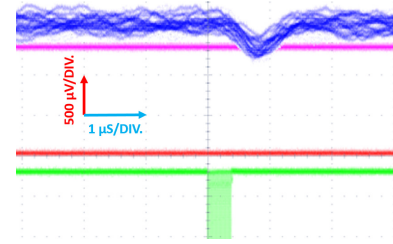


Figure 7: Oscilloscope picture of the response of the Nb/Al-STJ processed on the SOI wafer to 465nm pulsed laser light illumination in the range of $1 \mu\text{s}/\text{DIV}$ horizontal and $500 \mu\text{V}/\text{DIV}$ vertical. The trigger pulses from the laser pulser controller are shown together.

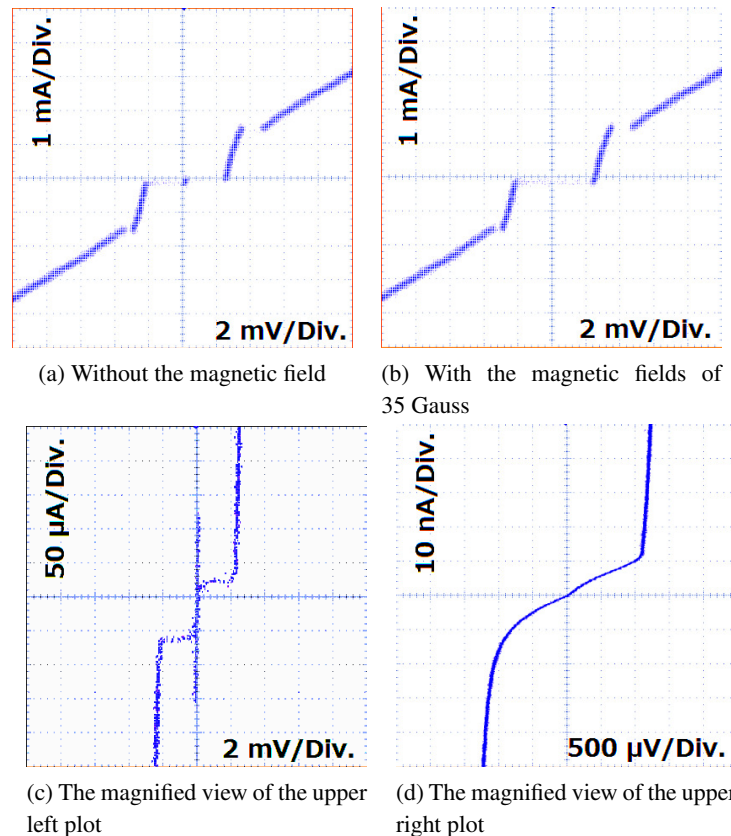


Figure 8: I-V curves of the Nb/Al-STJ processed on the SOI wafer.

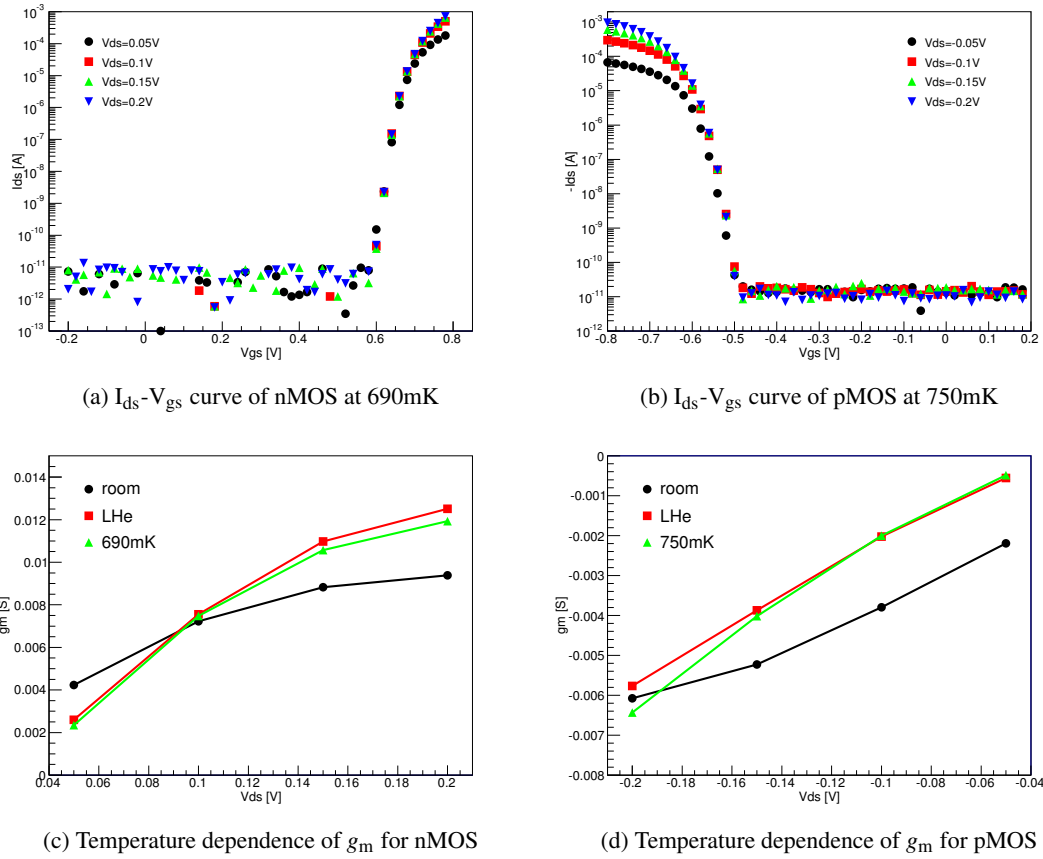


Figure 9: I_{ds} - V_{gs} curves of SOI-FET (width = $100 \times 10\mu\text{m}$, length= $1\mu\text{m}$) after processing the Nb/Al-STJ.

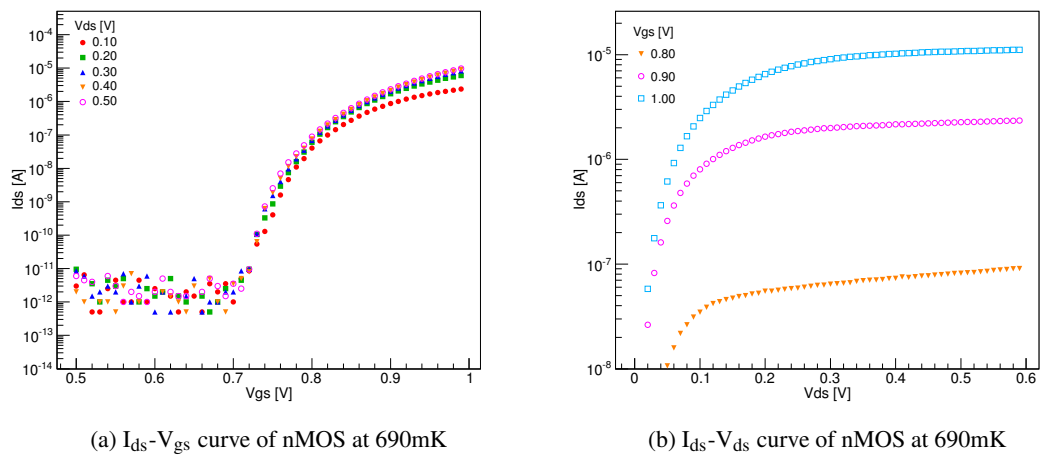


Figure 10: I_{ds} - V_{gs} curves of SOI-FET (width= $1.42\mu\text{m}$, length= $0.42\mu\text{m}$) after processing the Nb/Al-STJ.

5. Conclusion

The Nb/Al-STJ photon detector for detecting the far-infrared single photon is under development to search for the radiative decays of the cosmic background neutrino. To satisfy our requirements for the photon detector, we adopt the preamplifier operates at an ultra-low temperature. We processed the Nb/Al-STJ on the SOI preamplifier board directly, and examine the SOI-FETs at the ultra-low temperature as well as the Nb/Al-STJ processed on SOI wafer. Both of nMOS and pMOS indicated an excellent performance below 800mK and the Nb/Al-STJ processed on SOI board also showed to be of the nominal quality. SOI-STJ consequently can be a candidate for the detector.

Acknowledgments

We thank the detector technology project at KEK for maintaining equipment in the clean room. We thank Y.Otsuka at University of Tsukuba for lending us the dilution refrigerator kindly.

References

- [1] J. Beringer *et al.* (Particle Data Group), Phys. Rev. D86 (2012) 010001
- [2] P. B. Pal and L. Wolfenstein, Phys. Rev. D25 (1982) 766
- [3] M. A. B. Beg and W. J. Marciano, Phys. Rev. D17 1395 (1978)
- [4] S. H. Kim, K. Takemasa, Y. Takeuchi, S. Matsuura, J. Phys. Soc. Jpn., 81 (2012) 024101
- [5] S. H. Kim *et al.*, JPS Conf. Proc. 1, 013127 (2014)
- [6] T. Wada *et al.*, J. Low. Temp. Phys. 167, (2012) 602

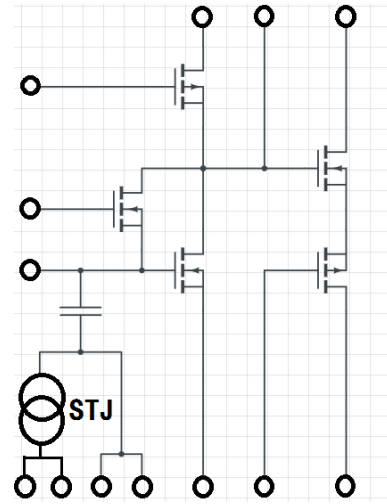


Figure 11: Design of the next version of SOI-STJ.